Quantitative Piezospectroscopy of the Ground and Excited States of Acceptors in Silicon*

H. R. Chandrasekhar, P. Fisher, A. K. Ramdas, and S. Rodriguez
Department of Physics, Purdue University, West Lafayette, Indiana 47907
(Received 8 June 1973)

A piezospectroscopic study of the excitation lines from the Γ_8 ground state to the first two Γ_8 excited states of the $p_{3/2}$ series of boron, aluminum, and indium (lines 1 and 2) and to the first Γ_6 excited state of boron ($2p'$ line) has been made for compressive force $\vec{F}$ along <111>, <100>, and <110>. The shear deformation-potential constants of the excited states and the ground state of Γ_8 symmetry have been determined from these measurements. The results for boron acceptors, taken together with the theoretical calculations of Bir, Butikov, and Pikus, yield the shear deformation-potential constants of the valence band of silicon, viz., $b = -1.92 \pm 0.05$ eV and $d = -4.84 \pm 0.10$ eV. Level-crossing effects have been observed associated with the $\Gamma_5 + \Gamma_6$ sublevels of the excited states of lines 1 and 2 for $\vec{F} \parallel$ <111>; nonlinear dependence on stress and stress-dependent intensity changes have been observed for the stress-induced components which have these $\Gamma_5 + \Gamma_6$ final states. These features have been accounted for on the basis of a perturbation theory used in conjunction with the results of Rodriguez, Fisher, and Barra. For the three acceptors investigated, the ground-state splitting as a function of stress is found to be the same for $\vec{F} \parallel$ <111>, <100>, or <110>. The expression for the splitting of a Γ_8 state for an arbitrary direction of compression shows that the extrema of the splitting occur for <111>, <100>, and <110>. The experimental results imply a ground-state splitting which is isotropic with respect to the direction of F, this isotropy being tested under the most stringent condition.

I. INTRODUCTION

The photoexcitation spectra of group-V donors and group-III acceptors in silicon and germanium have provided valuable information about the energy levels associated with these impurities.[1,2] Symmetries[2] as well as the magnetic quantum numbers and the deformation-potential constants characterizing the energy levels have been obtained from studies of the spectra under an external magnetic field[2-4] or a uniaxial stress.[2,5-7] To the extent these energy levels are describable in terms of the parameters characterizing the band extrema with which they are associated,[1] these studies yield information about the host crystal. Recently, a determination of the shear deformation-potential constant Ξ_u of the $\langle 100 \rangle$ conduction-band minima of silicon was made from a quantitative piezospectroscopic study of the excitation spectra of phosphorus, arsenic, antimony, and magnesium donors.[5] The purpose of this paper is to present and discuss the results of a similar investigation on the group-III acceptors, boron, aluminum, and indium in silicon.

II. EXPERIMENTAL PROCEDURE

The single-beam double-pass grating monochromator (model No. 99G) with the associated entrance and exit optics used in the present investigation has been described elsewhere.[8] A Perkin-Elmer wire-grid polarizer with AgBr substrate[9] was employed for wavelengths below ~20 μm. A "pile-of-plates" polyethylene polarizer[10] or a Perkin-Elmer wire-grid polarizer with polyethylene substrate[9] was used for wavelengths above ~17 μm. The quantitative-stress cryostat and details of sample preparation have been described in a recent publication.[5] All the measurements were made using liquid helium as a coolant. The optical samples were obtained from single-crystal ingots of silicon appropriately doped with the impurity of interest, viz., boron, aluminum, or indium[11]; the room-temperature carrier concentrations were ~10^{15} cm^{-3}.

III. THEORY

A substitutional neutral group-III acceptor in a group-IV semiconductor has energy levels which can be classified according to the double-valued irreducible representations of its site-symmetry group T_d, viz., Γ_6, Γ_7, or Γ_8.[12,13] Of these, Γ_6 and Γ_7 are doublets, whereas Γ_8 is a quadruplet. The top of the valence band for silicon and germanium, referred to as the $p_{3/2}$ band, belongs to Γ_8^+ of $\overline{O}_h$; below this, separated by the spin-orbit interaction, lies the top of the so-called $p_{1/2}$ band with Γ_7^+ symmetry.[14] In the effective-mass approximation[1] the ground state of the acceptor is a $\Gamma_8(T_d)$ level.[15] Electric dipole transitions are allowed from the Γ_8 ground state to any of the excited states.[16] Transitions from the ground state to the excited states associated with the $p_{3/2}$ ($p_{1/2}$) valence-band maximum will be referred to as the $p_{3/2}$ ($p_{1/2}$) series; these are shown schematically in Fig. 1.

The application of a uniaxial stress reduces the

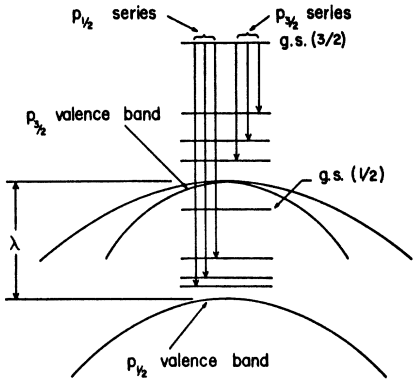

FIG. 1. Acceptor states associated with the valence band of silicon. Here g.s. is the ground state and λ is the separation of the $p_{3/2}$ valence band from the $p_{1/2}$ valence band at $\vec{k}=0$.

site symmetry and thus the degeneracy of the acceptor levels may be partially removed. The hole bound to the acceptor impurity is now subject to an additional field produced by the resultant homogeneous strain; to first order in the components of the strain tensor ϵ_{ij}, the additional potential is[17]

$$V=\sum_{i,j} V_{ij}\epsilon_{ij} \quad , \tag{1}$$

where $i,j=x,y$, or z, the cubic axes of the crystal. States belonging to Γ_6 are shifted isotropically by

$$\Delta E(\Gamma_6)=A(\epsilon_{xx}+\epsilon_{yy}+\epsilon_{zz})=A(s_{11}+2s_{12})T \quad , \tag{2}$$

where the deformation-potential constant A is given by $\frac{1}{3}\langle\psi_1|V_{xx}+V_{yy}+V_{zz}|\psi_1\rangle$, the s_{ij}'s are the elastic-compliance constants, and T is the applied force $\vec{F}$ per unit area and defined to be negative for compression. The wave function ψ_1 and its partner ψ_2 form a basis for Γ_6; the matrix representation of V in this basis is a multiple of the unit matrix.[18] A similar result holds for a Γ_7 level. For a Γ_8 level, V has the matrix form given by[17]

$$[V]=aI\sum_i \epsilon_{ii}+bP+\frac{2d}{\sqrt{3}}Q \quad , \tag{3}$$

$$P=\sum_i \epsilon_{ii}\left(J_i^2-\tfrac{5}{4}I\right) \quad , \tag{4}$$

$$Q=\sum_{i<j}\{J_iJ_j\}\epsilon_{ij} \quad , \tag{5}$$

where J_i are the components of the 4×4 angular momentum matrices; I is the 4×4 unit matrix; a, b, and d are deformation potential constants; and $\{J_iJ_j\}=\frac{1}{2}(J_iJ_j+J_jJ_i)$. By virtue of the Kramers theorem, the eigenvalues of $[V]$ in Eq. (3) occur in pairs. We now derive an expression for the energy separation between the two doublets resulting from the application of a uniaxial stress. The first term in Eq. (3) gives the shift of the center of gravity of the two doublets since the trace of the second and third terms vanish.[19] Let

$$W=bP+(2d/\sqrt{3})Q \quad . \tag{6}$$

The eigenvalues of W for an arbitrary strain are $\pm\frac{1}{2}\Delta$, where Δ is the energy separation of the two doublets. The secular polynomial associated with the eigenvalue problem for W is therefore

$$F(E)=\det[W_{kl}-E\delta_{kl}]=(E^2-\tfrac{1}{4}\Delta^2)^2 \quad , \tag{7}$$

since all its coefficients are invariant under a similarity transformation; here $k,l=1,2,3$, or 4. Since $\Delta^2=-(d^2F/dE^2)_{E=0}$ and

$$\frac{d^2F}{dE^2}=2\sum_{i<j}\begin{vmatrix} W_{ii}-E & W_{ij} \\ W_{ji} & W_{jj}-E \end{vmatrix} , \tag{8}$$

we obtain

$$\Delta^2=\mathrm{Tr}(W^2)-[\mathrm{Tr}(W)]^2=\mathrm{Tr}(W^2) \quad . \tag{9}$$

This quantity can be calculated as follows:

$$\mathrm{Tr}(W^2)=b^2\,\mathrm{Tr}(P^2)+(\tfrac{4}{3}d^2)\,\mathrm{Tr}(Q^2)+(4bd/\sqrt{3})\,\mathrm{Tr}(PQ) \quad . \tag{10}$$

It can be shown that

$$\mathrm{Tr}(P^2)=2[(\epsilon_{xx}-\epsilon_{yy})^2+(\epsilon_{yy}-\epsilon_{zz})^2+(\epsilon_{zz}-\epsilon_{xx})^2] \quad , \tag{11}$$

$$\mathrm{Tr}(Q^2)=3(\epsilon_{xy}^2+\epsilon_{yz}^2+\epsilon_{zx}^2) \quad , \tag{12}$$

and

$$\mathrm{Tr}(PQ)=0 \quad . \tag{13}$$

Thus,

$$\begin{aligned}\Delta^2 &= 2b^2[(\epsilon_{xx}-\epsilon_{yy})^2+(\epsilon_{yy}-\epsilon_{zz})^2+(\epsilon_{zz}-\epsilon_{xx})^2] \\ &\quad +4d^2(\epsilon_{xy}^2+\epsilon_{yz}^2+\epsilon_{zx}^2)=2b^2(s_{11}-s_{12})^2 \\ &\quad \times\{(\sigma_{xx}-\sigma_{yy})^2+(\sigma_{yy}-\sigma_{zz})^2+(\sigma_{zz}-\sigma_{xx})^2\} \\ &\quad +4d^2(\tfrac{1}{2}s_{44})^2(\sigma_{xy}^2+\sigma_{yz}^2+\sigma_{zx}^2) \quad .\end{aligned} \tag{14}$$

For uniaxial stress with $\vec{F}$ along an axis whose direction cosines are α_x, α_y, and α_z, the components of the stress tensor are $\sigma_{ij}=T\alpha_i\alpha_j$. Then

$$\Delta^2(\alpha_x,\alpha_y,\alpha_z)=\Delta_{100}^2+3(\Delta_{111}^2-\Delta_{100}^2)K(\alpha_x,\alpha_y,\alpha_z) \quad , \tag{15}$$

where $\Delta_{100}=2b(s_{11}-s_{12})T$, $\Delta_{111}=(d/\sqrt{3})s_{44}T$, and $K(\alpha_x,\alpha_y,\alpha_z)=\alpha_x^2\alpha_y^2+\alpha_y^2\alpha_z^2+\alpha_z^2\alpha_x^2$; $|\Delta_{100}|$ and $|\Delta_{111}|$ are the energy separations of the doublets for $\vec{F}\parallel\langle100\rangle$ and $\vec{F}\parallel\langle111\rangle$, respectively. It is interesting to note that if $|\Delta_{100}|=|\Delta_{111}|$, then $\Delta(\alpha_x,\alpha_y,\alpha_z)$ is the same for any direction of uniaxial stress; we shall refer to this as stress isotropy. The extrema of K occur for $\vec{F}\parallel\langle111\rangle$, $\langle110\rangle$, and $\langle100\rangle$, these being $\frac{1}{3}$, $\frac{1}{4}$, and 0, respectively.

In Fig. 2 are shown the splittings of the $\Gamma_8\rightarrow\Gamma_8$, $\Gamma_8\rightarrow\Gamma_6$, and $\Gamma_8\rightarrow\Gamma_7$ transitions for $\vec{F}\parallel\langle111\rangle$ and $\vec{F}\parallel\langle100\rangle$. The figure also shows the selection rules for electric dipole transitions. The ordering of

TABLE I. Symmetries, eigenvalues, and eigenfunctions of stress-induced sublevels of a Γ_8 state for $\vec{F} \parallel \langle 111 \rangle$ and $\langle 100 \rangle$.

Direction of $\vec{F}$	State	Eigenvalue[a]	Eigenfunction[b]
$\langle 111 \rangle$	$\Gamma_5+\Gamma_6(\bar{C}_{3v})$	$a(s_{11}+2s_{12})T+(d/2\sqrt{3})s_{44}T$	$\Lambda_{\pm 3/2}$
	$\Gamma_4(\bar{C}_{3v})$	$a(s_{11}+2s_{12})T-(d/2\sqrt{3})s_{44}T$	$\Lambda_{\pm 1/2}$
$\langle 100 \rangle$	$\Gamma_6(\bar{D}_{2d})$	$a(s_{11}+2s_{12})T+b(s_{11}-s_{12})T$	$\Psi_{\pm 3/2}$
	$\Gamma_7(\bar{D}_{2d})$	$a(s_{11}+2s_{12})T-b(s_{11}-s_{12})T$	$\Psi_{\pm 1/2}$

[a]Following G. E. Pikus and G. L. Bir {Fiz. Tverd. Tela 1, 1642 (1959) [Sov. Phys.-Solid State 1, 1502 (1960)]}, the eigenvalues are those of the bound hole; W. H. Kleiner and L. Roth [Phys. Rev. Lett. 2, 334 (1959)] use electron energy. The definitions of the deformation potential constants of the latter are related to those of the former by $D_u=-(\frac{2}{3})b$ and $D'_u=-(\frac{1}{2}\sqrt{3})d$.

[b]See Eqs. (1), (2), (9), and (22) of Ref. 17.

the stress induced sublevels for the Γ_8 ground state and the Γ_8 excited states of lines 1 and 2 are chosen on the basis of the polarization features and depopulation effects as discussed in an earlier publication.[15] Table I presents the eigenvalues and eigenfunctions for the Γ_8 states with $\vec{F} \parallel \langle 111 \rangle$ or $\langle 100 \rangle$. Note for $\vec{F} \parallel \langle 111 \rangle$, the lower sublevel of the excited state of line 2 and the upper sublevel of the excited state of line 1 are of the same symmetry, $\Gamma_5+\Gamma_6$, and will cross at sufficiently large stresses. (A similar situation can occur for $\vec{F} \parallel \langle 100 \rangle$ as shown in Fig. 2 and for $\vec{F} \parallel \langle 110 \rangle$, where all the stress induced sublevels have Γ_5 symmetry of $\bar{C}_{2v}$.) Under these conditions the two $(\Gamma_5+\Gamma_6)$ states can interact or mix via the strain potential. Following the notation of Ref. 17, the eigenfunctions of the $\Gamma_5+\Gamma_6$ levels are designated by $\Lambda^{(i)}_{\pm 3/2}$, where $i=1$ or 2 according as the final state corresponds to line 1 or 2. The matrix elements of the Hamiltonian including V in these four states is given in Table II. In this table

$$V_{ii}^{(3/2)} = a_i(s_{11}+2s_{12})T+(d_i/2\sqrt{3})s_{44}T, \quad i=1,2 \qquad (16)$$

and

$$V_{12} = \langle \Lambda^{(1)}_{3/2} | V | \Lambda^{(2)}_{3/2} \rangle = \langle \Lambda^{(1)}_{-3/2} | V | \Lambda^{(2)}_{-3/2} \rangle \ . \qquad (17)$$

The last equality in Eq. (17) follows from the time-reversal invariance of V, and E_1 and E_2 are the zero-stress positions of lines 1 and 2. The eigenvalues of the Hamiltonian including the interaction are $\frac{1}{2}(E_1+E_2+V_{11}^{(3/2)}+V_{22}^{(3/2)})\pm R$, where

$$R=\tfrac{1}{2}[(E_2-E_1+V_{22}^{(3/2)}-V_{11}^{(3/2)})^2+4|V_{12}|^2]^{1/2} \ . \qquad (18)$$

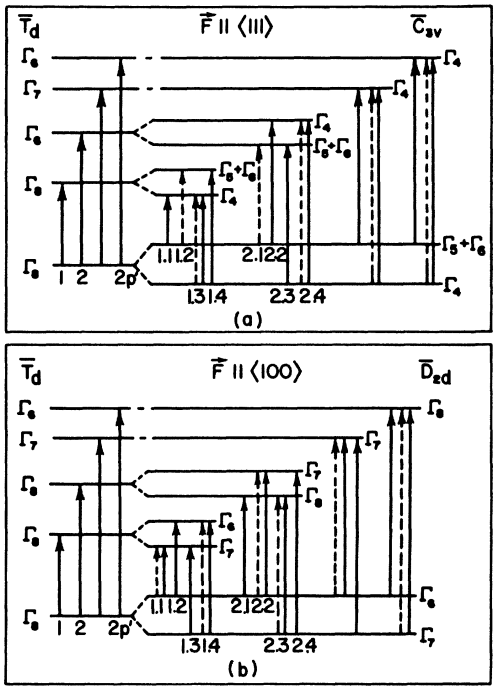

FIG. 2. Allowed transitions from a Γ_8 ground state to Γ_6, Γ_7, and Γ_8 excited states of the double group $\bar{T}_d$ with compressive force $\vec{F}$ along $\langle 111 \rangle$ or $\langle 100 \rangle$. The site symmetry is C_{3v} and D_{2d} for the $\langle 111 \rangle$ and $\langle 100 \rangle$ compressions, respectively; the designations next to the levels denote the irreducible representations of the appropriate double point group following the notation of Ref. 12. The dashed arrows are for the electric vector $\vec{E} \parallel \vec{F}$ while the full arrows are for $\vec{E} \perp \vec{F}$. Transitions labeled 1 and 2 correspond to the first two lines in the $p_{3/2}$ series, whereas $2p'$ refers to the first of the $p_{1/2}$ series. (See Ref. 15.)

TABLE II. Matrix elements of the Hamiltonian, including the strain potential V, between the $\Gamma_5+\Gamma_6$ final states of lines 1 and 2.

	$\Lambda^{(1)}_{3/2}$	$\Lambda^{(1)}_{-3/2}$	$\Lambda^{(2)}_{3/2}$	$\Lambda^{(2)}_{-3/2}$
$\Lambda^{(1)}_{3/2}$	$E_1+V_{11}^{(3/2)}$	0	V_{12}	0
$\Lambda^{(1)}_{-3/2}$	0	$E_1+V_{11}^{(3/2)}$	0	V_{12}
$\Lambda^{(2)}_{3/2}$	V_{12}^*	0	$E_2+V_{22}^{(3/2)}$	0
$\Lambda^{(2)}_{-3/2}$	0	V_{12}^*	0	$E_2+V_{22}^{(3/2)}$

The corresponding eigenfunctions are

$$\Lambda^{(+)}_{\pm 3/2} = \sin\tfrac{1}{2}\theta\,\Lambda^{(1)}_{\pm 3/2} - \cos\tfrac{1}{2}\theta\, e^{i\varphi}\,\Lambda^{(2)}_{\pm 3/2} \qquad (19)$$

and

$$\Lambda^{(-)}_{\pm 3/2} = \cos\tfrac{1}{2}\theta\,\Lambda^{(1)}_{\pm 3/2} + \sin\tfrac{1}{2}\theta\, e^{i\varphi}\,\Lambda^{(2)}_{\pm 3/2}\ . \qquad (20)$$

Here the angles θ and φ are defined such that

$$R\cos\theta = \tfrac{1}{2}(E_2 - E_1 + V_{22}^{(3/2)} - V_{11}^{(3/2)}) \qquad (21)$$

and

$$R\sin\theta\, e^{-i\varphi} = -V_{12}\ . \qquad (22)$$

The superscripts + and − in Eqs. (19) and (20) correspond to $\pm R$ in the eigenvalues.

The new features in the relative intensities arising from the mixing of states discussed above are incorporated by calculating the matrix elements from the ground-state multiplet to the excited-state multiplets of lines 1 and 2. In this procedure we use the wave functions $\Lambda^{(+)}_{\pm 3/2}$ and $\Lambda^{(-)}_{\pm 3/2}$ given in Eqs. (19) and (20) instead of $\Lambda^{(2)}_{\pm 3/2}$ and $\Lambda^{(1)}_{\pm 3/2}$, respectively; $\Lambda^{(2)}_{\pm 1/2}$ and $\Lambda^{(1)}_{\pm 1/2}$ remain the same. We obtain a 8×4 transition matrix in a manner similar to that given in Ref. 17, p. 2226 using parameters similar to those in this reference, with subscripts 1 and 2 corresponding to lines 1 and 2, respectively.[20] These results are shown in Table III. In constructing this table, we have assumed that the relative phases of the wave functions associated with the excited states of lines 1 and 2 are not correlated.

IV. EXPERIMENTAL RESULTS AND DISCUSSION

Onton *et al.*[15] (hereafter referred to as OFR) have reported the $p_{3/2}$ and the $p_{1/2}$ spectra of boron, aluminum, gallium, and indium acceptors in silicon corresponding to a large number of excited states. They have also studied many of these lines under uniaxial stress and deduced the symmetries of the ground and the excited states on the basis of the dichroism of the stress-induced components; however, these results were qualitative in that the magnitude of the stress was not known. Here we give results for the lines 1 and 2 of the $p_{3/2}$ series of boron, aluminum, and indium and for the $2p'$ line of boron obtained with the quantitative stress cryostat referred to in Sec. II.

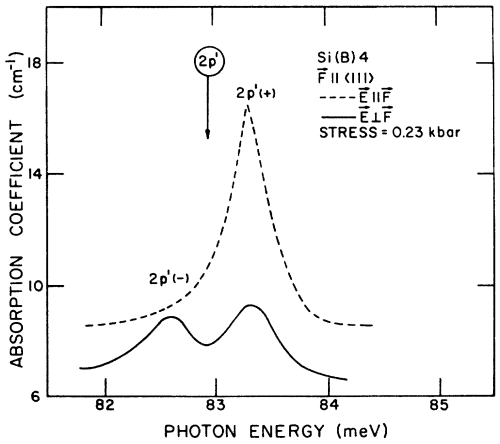

FIG. 3. Effect of uniaxial stress on the $2p'$ line of boron acceptors in silicon with $\vec{F} \parallel \langle 111\rangle$. Room-temperature resistivity $\sim 4\ \Omega$ cm. The encircled number with the vertical arrow, in this and the following figures, designates the zero-stress position of the line.

A. Boron

Shown in Fig. 3 is the $2p'$ line of boron acceptors in silicon with $\vec{F} \parallel \langle 111\rangle$. On the basis of a piezospectroscopic study, OFR ascribed this line to the transition from the $\Gamma_8(p_{3/2})$ ground state to an excited state of Γ_6 or Γ_7 symmetry associated with the $p_{1/2}$ valence band. The two components labeled $2p'(+)$ and $2p'(-)$ are due to the splitting of the Γ_8 ground state into a doublet; the $2p'(-)$ component

TABLE III. Relative intensities for stress-induced components of lines 1 and 2 including interaction of $\Gamma_5+\Gamma_6$ sublevels ($\vec{F} \parallel \langle 111\rangle$).

Zero-stress transition	Stress-induced components	Relative intensity $\vec{E} \parallel \vec{F}$	Relative intensity $\vec{E} \perp \vec{F}$
$\Gamma_8 \rightarrow \Gamma_8$ (line 1)	$\Gamma_4 \rightarrow \Gamma_4$ (1.3)	$\frac{1}{2}N_1(1-u_1)$	$\frac{1}{2}N_1u_1$
	$\Gamma_4 \rightarrow \Gamma_5+\Gamma_6$ (1.4)	0	$N_1(\frac{1}{2}-\frac{1}{4}u_1)\cos^2\frac{1}{2}\theta + N_2(\frac{1}{2}-\frac{1}{4}u_2)\sin^2\frac{1}{2}\theta$
	$\Gamma_5+\Gamma_6 \rightarrow \Gamma_4$ (1.1)	0	$N_1(\frac{1}{2}-\frac{1}{4}u_1)$
	$\Gamma_5+\Gamma_6 \rightarrow \Gamma_5+\Gamma_6$ (1.2)	$\frac{1}{2}N_1(1+u_1)\cos^2\frac{1}{2}\theta + \frac{1}{2}N_2(1+u_2)\sin^2\frac{1}{2}\theta$	0
$\Gamma_8 \rightarrow \Gamma_8$ (line 2)	$\Gamma_4 \rightarrow \Gamma_4$ (2.4)	$\frac{1}{2}N_2(1-u_2)$	$\frac{1}{2}N_2u_2$
	$\Gamma_4 \rightarrow \Gamma_5+\Gamma_6$ (2.3)	0	$N_1(\frac{1}{2}-\frac{1}{4}u_1)\sin^2\frac{1}{2}\theta + N_2(\frac{1}{2}-\frac{1}{4}u_2)\cos^2\frac{1}{2}\theta$
	$\Gamma_5+\Gamma_6 \rightarrow \Gamma_4$ (2.2)	0	$N_2(\frac{1}{2}-\frac{1}{4}u_2)$
	$\Gamma_5+\Gamma_6 \rightarrow \Gamma_5+\Gamma_6$ (2.1)	$\frac{1}{2}N_1(1+u_1)\sin^2\frac{1}{2}\theta + \frac{1}{2}N_2(1+u_2)\cos^2\frac{1}{2}\theta$	0

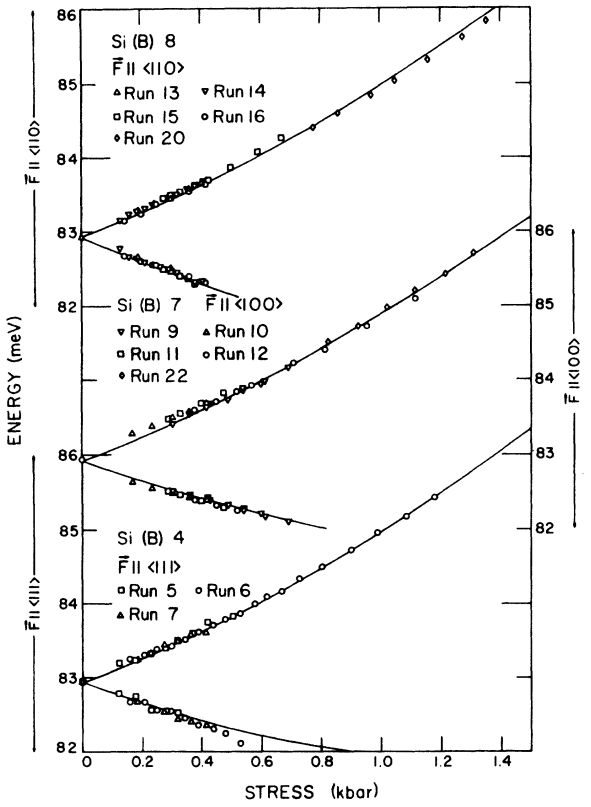

FIG. 4. Stress dependence of the components of the $2p'$ line of boron acceptors in silicon for $\vec{F} \parallel \langle 111 \rangle$, $\langle 100 \rangle$, or $\langle 110 \rangle$. Room-temperature resistivities of the specimens used were Si(B)4 and 8 ~4 Ω cm; Si(B)7 ~1 Ω cm. For each direction of compression, the solid curves passing through the positions of the high-energy components represent the second-degree polynomial $E(2p') + G|T| + H|T|^2$; $E(2p')$ is the zero-stress position, G and H are constants, and $|T|$ is the magnitude of the stress. The curve passing through the positions of the low-energy components represents $E(2p') - G|T| + H|T|^2$. The polynomial fits were obtained by the method of least squares.

shows a decrease in intensity with increasing stress as a consequence of the depopulation of the stress-induced upper sublevel of the ground state. As expected, the $2p'(+)$ component shows a corresponding increase in intensity. Similar results are obtained for $\vec{F} \parallel \langle 100 \rangle$ and $\vec{F} \parallel \langle 110 \rangle$. The ordering of the stress induced sublevels of the ground state for $\vec{F} \parallel \langle 111 \rangle$ in Fig. 2 is deduced from the polarization and depopulation effects of $2p'(+)$ and $2p'(-)$; this ordering is independent of whether the final state is a Γ_6 or Γ_7 level. However, for $\vec{F} \parallel \langle 100 \rangle$ the ordering shown in Fig. 2 is consistent with the behavior of the $2p'$ line provided the final state is a Γ_6 level.

The positions of the $2p'(+)$ and the $2p'(-)$ components as a function of stress are shown in Fig. 4 for $\vec{F} \parallel \langle 111 \rangle$, $\langle 100 \rangle$, and $\langle 110 \rangle$. The solid line passing through the positions of $2p'(+)$ represents a second-degree polynomial fit by the method of least squares to the data, i.e., $E[2p'(+)] = E(2p') + G|T| + H|T|^2$, where $E(2p')$ is the zero-stress position of the $2p'$ line and G and H are constants. The curve passing through the data points for $2p'(-)$ represents $E(2p') - G|T| + H|T|^2$. The spacing between the stress-induced sublevels of the Γ_8 ground state $\Delta = E[2p'(+)] - E[2p'(-)] = 2G|T|$, as a function of stress ($|T|$), is shown in Fig. 5 for $\vec{F} \parallel \langle 111 \rangle$, $\langle 100 \rangle$, and $\langle 110 \rangle$. The straight lines passing through the data points represent least-squares fits; it is clear that Δ is linear in stress. The slopes are 3.24 ± 0.11, 3.13 ± 0.14, and 3.31 ± 0.12 meV/kbar for $\vec{F} \parallel \langle 111 \rangle$, $\langle 100 \rangle$, and $\langle 110 \rangle$, respectively. The errors indicated here and in other similar determinations were obtained by adding the fractional errors in the determination of the cross-sectional area, in the calibration of force versus pressure and in the slope of Δ versus stress. It is interesting to note that the slopes given by the least-squares fits are equal, within experimental error, hence, $|\Delta_{111}| = |\Delta_{100}| = |\Delta_{110}|$. As pointed out in the previous section $|\Delta_{111}| = |\Delta_{100}|$ implies an isotropic splitting for a given compression irrespective of the direction in which $\vec{F}$ is applied. This aspect of the ground-state splitting has been

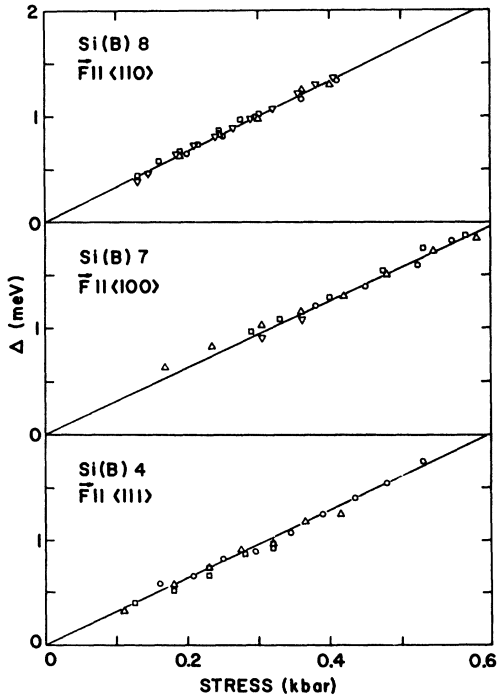

FIG. 5. Stress dependence of $\Delta = E[2p'(+)] - E[2p'(-)]$ for $\vec{F} \parallel \langle 111 \rangle$, $\langle 100 \rangle$, or $\langle 110 \rangle$ of boron acceptors in silicon. The straight lines passing through the data points represent least-squares fits. The symbols for data points are the same as in the corresponding parts of Fig. 4.

TABLE IV. Deformation-potential constants of the ground and excited states and the matrix element $|V_{12}|/|T|$ for acceptors in silicon.

Acceptor	b_0 (eV)	b_1 (eV)	b_2 (eV)	d_0 (eV)	d_1 (eV)	d_2 (eV)	$\|V_{12}\|/\|T\|$ (meV/kbar)
Boron	-1.61 ± 0.07	0.20 ± 0.15	1.61	-4.50 ± 0.15[a] -4.46 ± 0.1[b]	-2.31 ± 0.25	2.64 ± 0.25	1.83 ± 0.10
Aluminum	-1.43 ± 0.06	0.10 ± 0.05	1.43	-3.84 ± 0.12	-3.11 ± 0.22	2.56 ± 0.22	1.72 ± 0.10
Indium	-0.98 ± 0.03	~0	1.76 ± 0.10	-2.68 ± 0.15	-3.22 ± 0.25	3.54 ± 0.25	2.07 ± 0.10

[a]Deduced from $2p'$ line.

[b]Deduced from line 2.

previously deduced by OFR from the relative intensities of the two stress-induced components of the $2p'$ line.[21]

The deformation potential constants characterizing the Γ_8 ground state can now be deduced from the above results. With T defined to be negative for compression and using the known elastic compliance constants s_{ij},[22] the ordering of the ground-state sublevels given in Fig. 2, implies a negative sign for the ground-state deformation-potential constants b_0 and d_0. The values deduced from Fig. 5 are given in Table IV. The values for G obtained from the polynomial fits of Fig. 4 and the least-squares fits of Fig. 5 agree very well. The constant H in the polynomial fit of the data in Fig. 4 is 0.54 ± 0.02, 0.48 ± 0.04, and 0.33 ± 0.02 meV/kbar^2 for $\vec{F}\parallel\langle111\rangle$, $\langle100\rangle$, and $\langle110\rangle$, respectively. The deformation-potential theory which includes terms only linear in strain will not give such a nonlinear effect. We have not investigated the origin of this term which physically represents a shift of the center of gravity of the sublevels of the ground state and/or a shift of the excited state, the combined effect being nonlinear in stress.

In Fig. 6 we show the stress-induced components for lines 1 and 2 of boron acceptors in silicon for $\vec{F}\parallel\langle111\rangle$ at two different stresses. The spectra were recorded with the electric vector of the radiation $\vec{E}$ either parallel or perpendicular to $\vec{F}$. Lines 1 and 2 arise from the ground state to the first two Γ_8 excited states of the $p_{3/2}$ series. The ordering of the stress-induced sublevels of the excited states of lines 1 and 2 as given in Fig. 2(a) follows OFR and is confirmed by the present results. We assume that the ordering of the Γ_8 ground-state sublevels is predetermined by the behavior of the $2p'$ line.

Figure 7 shows the positions of the stress induced components of lines 1 and 2 as a function of stress. The solid curves represent second-degree polynomial fits by the method of least squares. We note that the energy spacing between 2.3 and 2.1 as well as that between 2.4 and 2.2 yields the ground-state splitting. This spacing is plotted as a function of stress in Fig. 8; the straight line represents a least-squares fit through the data points and has a slope of 3.21 ± 0.10 meV/kbar, in excellent agreement with the value for this determined from the behavior of the $2p'$ line; Table IV includes the value for d_0 deduced from it. Similarly the spacing between 1.4 and 1.2 as well as that between 1.3 and 1.1 should correspond to the ground-state splitting; this is indeed found to be the case. However, due to the temperature used in these measurements the low intensity of 1.1 and 1.2, even for moderate stresses, prevented us from obtaining data for line 1 comparable in accuracy to that of line 2.

From Fig. 7 it is clear that the stress depen-

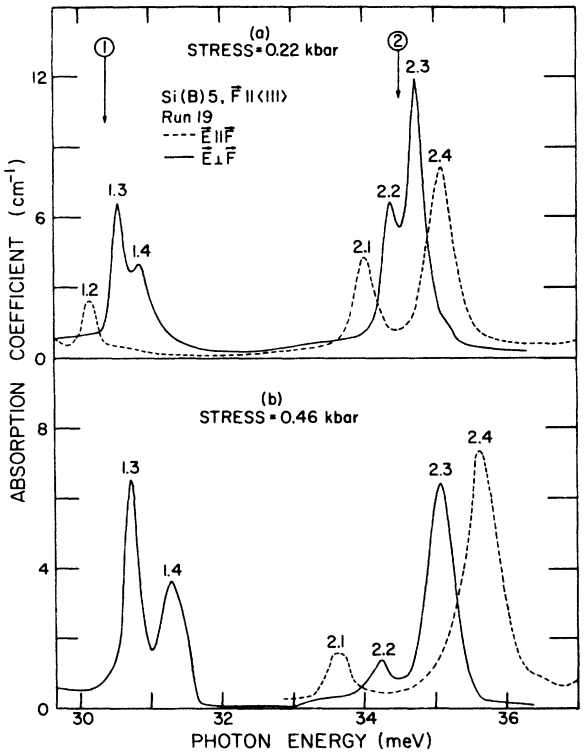

FIG. 6. Effect of a $\langle111\rangle$ compression on lines 1 and 2 of boron in silicon. Room-temperature carrier concentration $p(300\,^{\circ}\mathrm{K}) = 1.5\times10^{15}$ cm^{-3}.

dence of the positions of 1.4, 2.1, and 2.3 exhibits considerable nonlinearity. These components arise from transitions whose final states are of $\Gamma_5 + \Gamma_6$ symmetry. As can be appreciated from Fig. 2, these nonlinearities could be a manifestation of the stress-induced mixing effects discussed in Sec. III. The positions of 2.4, 2.3, 1.4, and 1.3 are given by

$$E_{2,4} = E_2 + V_{22}^{(1/2)} - V_{00}^{(1/2)} \ , \tag{23}$$

$$E_{2,3} = \tfrac{1}{2}(E_1 + E_2 + V_{11}^{(3/2)} + V_{22}^{(3/2)}) - R - V_{00}^{(1/2)} \ , \tag{24}$$

$$E_{1,4} = \tfrac{1}{2}(E_1 + E_2 + V_{11}^{(3/2)} + V_{22}^{(3/2)}) - R - V_{00}^{(1/2)} \ , \tag{25}$$

$$E_{1,3} = E_1 + V_{11}^{(1/2)} - V_{00}^{(1/2)} \ , \tag{26}$$

where

$$V_{ii}^{(1/2)} = a_i(s_{11} + 2s_{12})T - (d_i/2\sqrt{3})s_{44}T, \quad i = 0, 1, \text{ or } 2. \tag{27}$$

From Eqs. (23)–(27) and d_0 deduced earlier it is possible to determine the deformation potential constants d_1 and d_2 as well as $|V_{12}|/|T|$ which are given in Table IV. It should be noted that the available experimental data do not permit a determination of a_0, a_1, and a_2. It is seen in Fig. 7 that 1.3 and 2.4 show a small nonlinear stress dependence of the same magnitude. We believe that this is due to a nonlinear shift of the center of gravity of the ground state; in Eqs. (23)–(26), this common term is omitted.

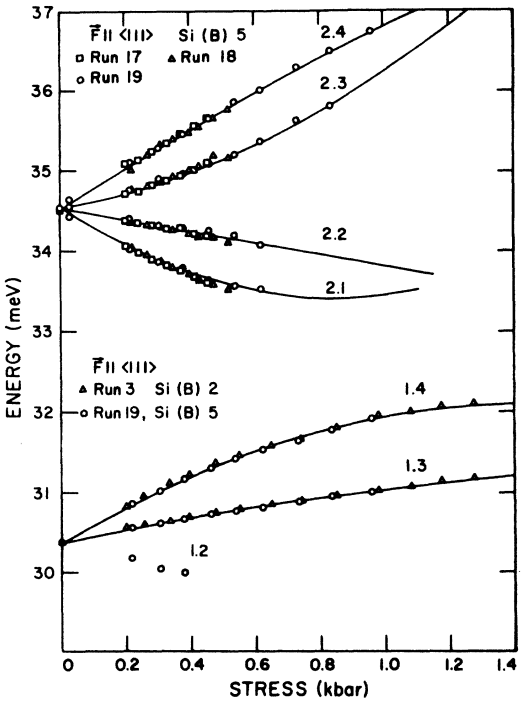

FIG. 7. Stress dependence of the energies of the components of line 1 and line 2 of boron in silicon for $\vec{F} \parallel \langle 111 \rangle$. The solid curves passing through the data points represent second-degree polynomial fits by the method of least squares.

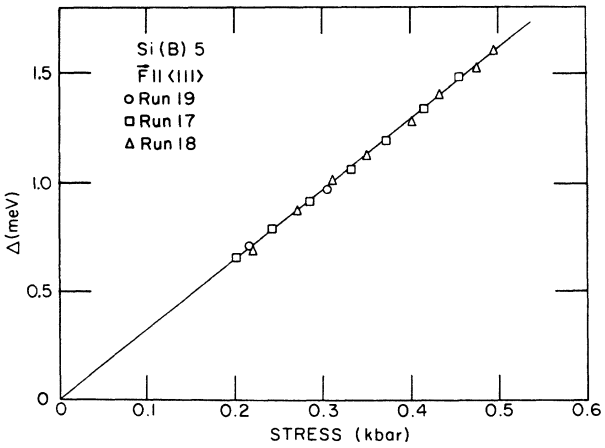

FIG. 8. Average of the energy spacing (2.4 – 2.2) and (2.3 – 2.1) as a function of stress as deduced from Fig. 7. The straight line passing through the data points represents a least-squares fit.

A comparison of Figs. 6(a) and 6(b) reveals unusual changes in the relative intensities of the stress-induced multiplets of lines 1 and 2; at the higher stress, 1.4 has decidedly increased in intensity, whereas 2.3 has decreased. The dramatic increase in the intensity of 1.4 at higher stresses can be clearly seen in Fig. 9, where 1.3 and 1.4 are shown for two stresses. Since 1.4 and 2.3 correspond to transitions from the Γ_4 sublevel of the ground state to the $\Gamma_5 + \Gamma_6$ sublevels of the excited states of lines 1 and 2, respectively, which mix under stress, the above behavior can be explained as discussed in Sec. III. In order to give a quantitative description of the above features we need to know u_1, u_2, N_1, N_2, and θ, the parameters defined in Sec. III and in Ref. 20. The values of N_1 and N_2 are given by the zero-stress intensities of lines 1 and 2; u_1 and u_2 are deduced from the relative intensities of the stress-induced multiplets of lines 1 and 2 at very low values of stress for which the mixing can be ignored. These values are $u_1 = 0.9 \pm 0.1$ and $u_2 = 0.1 \pm 0.1$. The errors are due to the difficulty in measuring the areas of relatively weak components and in correcting for depopulation effects since the sample temperature was not precisely known. Besides, at low stresses the components are not well resolved. Figure 10 shows the relative intensities of the stress-induced multiplets as a function of the mixing parameter θ. This figure was constructed from Table III for the values of $u_1 = 0.9$, $u_2 = 0.1$, $N_1 = 0.17$, and $N_2 = 0.83$. A comparison of the experimental results in Figs. 6 and 9 with the theoretical predictions in Fig. 10 shows a qualitative agreement. The following features are noteworthy: (i) 2.3 in $\vec{E} \perp \vec{F}$ is more in-

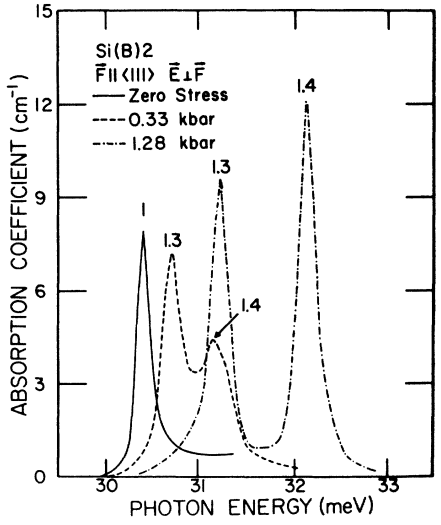

FIG. 9. Stress-induced changes in the relative intensities of the components 1.3 and 1.4 of boron acceptors in silicon with $\vec{F} \parallel \langle 111 \rangle$. The zero-stress line is shown with a solid curve and labeled 1.

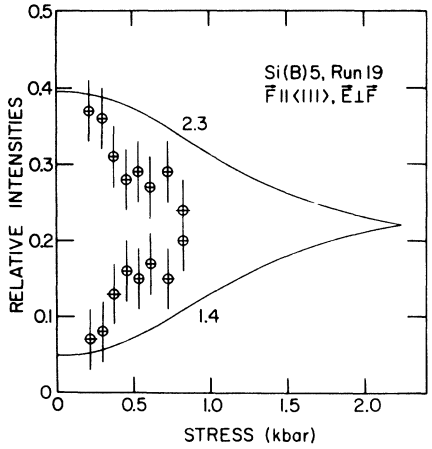

FIG. 11. Relative intensities of the components 2.3 and 1.4 for $\vec{F} \parallel \langle 111 \rangle$ as a function of stress. The intensity of each component at a given stress is computed as a fraction of the sum of the intensities of 2.3 and 1.4 normalized to 0.441; this corresponds to the theoretical value for this sum used for the solid curves in this figure and also in Fig. 10.

tense than 2.4 in $\vec{E} \parallel \vec{F}$ for small stresses but at large stresses it is weaker; (ii) 1.4 is weaker than 1.3 initially but becomes stronger at larger stresses; (iii) 2.1, corrected for the depopulation effect, is initially stronger than 2.4 at a stress smaller than that of Fig. 6(a), whereas the reverse is true at the higher stresses; (iv) the low intensity of 1.3 in $\vec{E} \parallel \vec{F}$ and of 2.4 in $\vec{E} \perp \vec{F}$ is consistent with the observations. In Fig. 11 we show the relative intensities of 1.4 and 2.3 as a function of stress rather than as a function of θ; qualitatively speaking the data points follow the theoretical curves shown as solid lines. The quantitative agreement is only fair; it is not clear at this stage whether this is due to some factors not included in

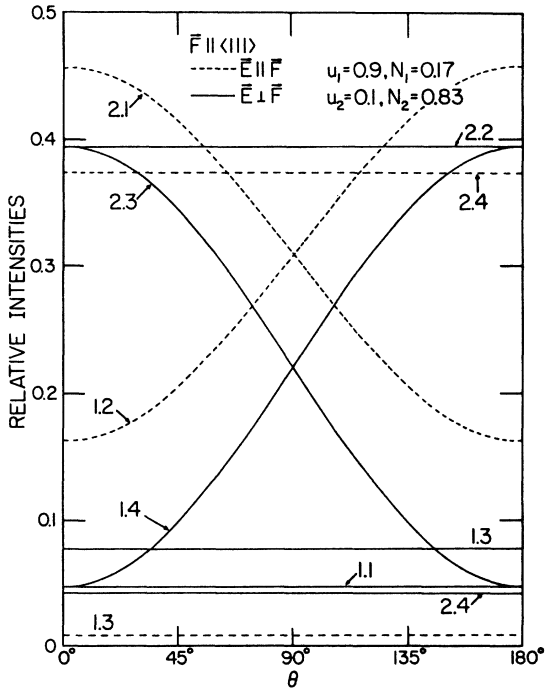

FIG. 10. Relative intensities of the stress-induced components of lines 1 and 2, including the effects due to the interaction of the $\Gamma_5+\Gamma_6$ final states, as a function of θ defined in Eqs. (21) and (22). The figure has been constructed from Table III for the values of u_1, u_2, N_1, and N_2 experimentally obtained for boron acceptors in silicon; these parameters have been defined in Ref. 20.

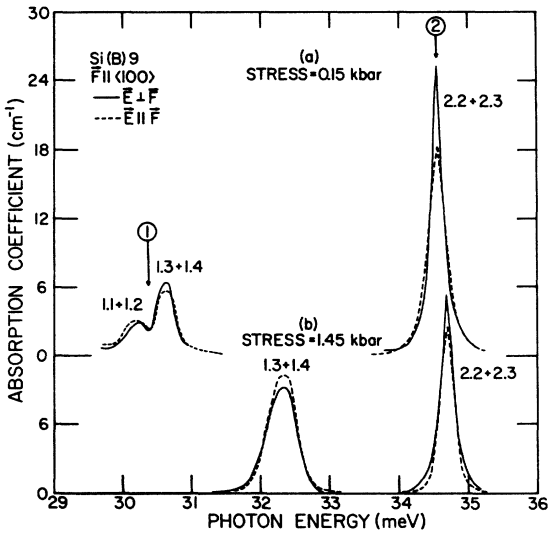

FIG. 12. Effect of a $\langle 100 \rangle$ compression on lines 1 and 2 of boron in silicon. $p(300\,^{\circ}\mathrm{K}) = 1.5 \times 10^{15}$ cm^{-3}.

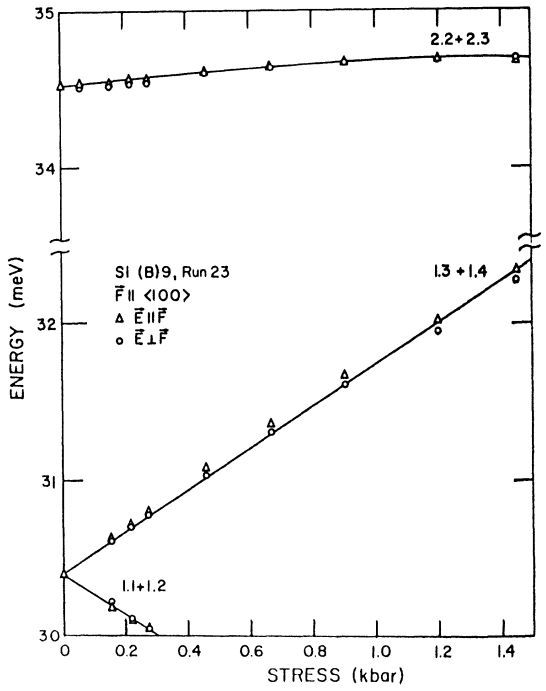

FIG. 13. Stress dependence of the energies of the stress-induced components of lines 1 and 2 of boron acceptors in silicon for $\vec{F} \parallel \langle 100 \rangle$. The solid straight lines passing through 1.3+1.4 as well as 1.1+1.2 represent least-squares fits. The solid curve passing through 2.2 +2.3 is a second-degree polynomial fit to the data.

the theory. For example, the experimental results appear to indicate an increase in $N_1 : N_2$ with increasing stress contrary to the assumption that it is a constant.

The results for lines 1 and 2 of boron acceptors in silicon with $\vec{F} \parallel \langle 100 \rangle$ are shown in Fig. 12 for two stresses. In Fig. 13 the positions of the stress-induced components are shown as a function of stress. The components 2.2 and 2.3 remained unresolved up to ~1.5 kbar and occurred very close to the zero-stress position of line 2. The polarization features are consistent with the level scheme shown for this line in Fig. 2(b), the excited-state splitting being almost equal to that of the ground state. Hence the deformation potential constant b_2 is equal in magnitude to b_0 but of the opposite sign, since the ordering of the excited state sublevels is opposite to that of the ground-state sublevels. The level scheme for line 2 is further supported by the fact that for $u_2 \sim 0.1$, $\Gamma_6 \rightarrow \Gamma_6$, and $\Gamma_7 \rightarrow \Gamma_7$ transitions have very small intensities as can be seen from Table XV of Ref. 17; the failure to observe 2.1 and 2.4 can thus be understood. The intensity of the line labeled 1.1 +1.2 in Fig. 13 decreases with increasing stress as a result of depopulation. Also the spacing between 1.3+1.4 and 1.1+1.2 is nearly equal to that of the ground state thus indicating that the excited state for line 1 splits very little compared to the ground state resulting in the coincidence of 1.1 with 1.2 and of 1.3 with 1.4. The straight lines passing through the data points for 1.1+1.2 and 1.3+1.4 represent least-squares fits; from the difference of their slopes it is deduced that the spacing between them increases linearly as 2.74 ± 0.15 meV/kbar. This is to be compared with 3.13 ± 0.14 meV/kbar, the rate at which the ground state splits as deduced from the behavior of the $2p'$ line. The spacing between the two components observed for $\vec{E} \parallel \vec{F}$ should give the sum of the splittings of the excited and the ground state. Since experimentally this is smaller than the ground-state splitting by ~10%, the level scheme proposed in Fig. 2(b) for line 2 may also represent the situation for line 1. If this were the case, the spacing between the two components observed for $\vec{E} \parallel \vec{F}$ would represent the *difference* in the ground-state and the excited-state splittings; with this interpretation b_1 is estimated to be 0.20 ± 0.15 eV (see Table IV).

The relative intensities of the stress-induced multiplet of a given line for $\vec{F} \parallel \langle 100 \rangle$ have been calculated by Rodriguez *et al.*[17]; these have been shown to depend on an additional parameter v besides u already defined for $\vec{F} \parallel \langle 111 \rangle$. From Table

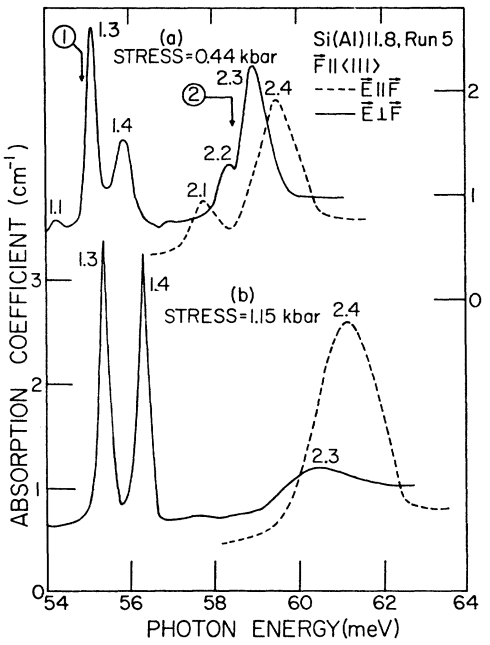

FIG. 14. Effect of a ⟨111⟩ compression on lines 1 and 2 of aluminum acceptors in silicon. $p(300\,^{\circ}\mathrm{K}) = 2.7 \times 10^{15}$ cm^{-3}. The somewhat larger widths of the components is due to a stress inhomogeneity present in this measurement and is more noticeable in 2.3 and 2.4 which have larger shifts.

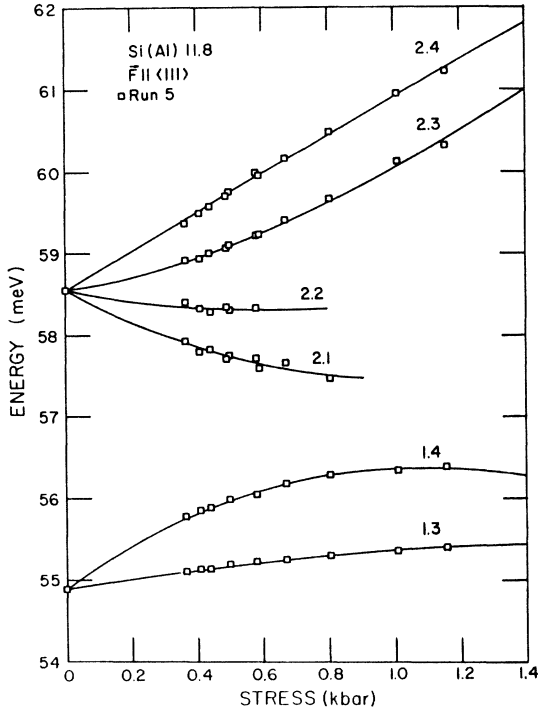

FIG. 15. Stress dependence of the energies of the components of lines 1 and 2 of aluminum acceptors in silicon for $\vec{F} \parallel \langle 111 \rangle$. The solid curves passing through the data points represent second-degree polynomial fits by the method of least squares.

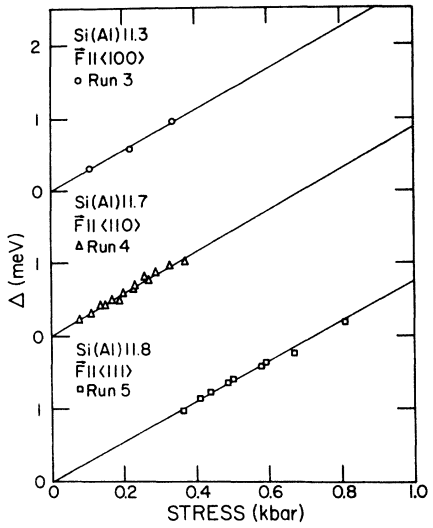

FIG. 16. Ground-state splitting Δ of aluminum acceptors in silicon as a function of stress with $\vec{F} \parallel \langle 111 \rangle$, $\langle 110 \rangle$, or $\langle 100 \rangle$. The values for Δ were determined from the energy spacing (2.4 − 2.2) and (2.3 − 2.1) for $\vec{F} \parallel \langle 111 \rangle$ from Fig. 15 and from the energy spacing (1.4 − 1.2) for $\vec{F} \parallel \langle 100 \rangle$ from Fig. 18; for $\vec{F} \parallel \langle 110 \rangle$, Δ was determined from the energy spacing (1.4 − 1.2) (see Fig. 19 for a typical spectrum).

XV of Ref. 17, taken together with the level scheme shown in Fig. 2(b), the intensity of 2.2 + 2.3 for $\vec{E} \parallel \vec{F}$ at low stress and at very high stress should be in the ratio $\frac{1}{2}$: $(\frac{1}{2} + v_2)$. From our data we thus estimate v_2 to be -0.1 ± 0.1. Similarly v_1 can be estimated from the relative intensities of 1.2 and 1.3 for $\vec{E} \parallel \vec{F}$ assuming the level scheme for the final states the same as for line 2, the ratio of the intensities of 1.2 and 1.3 should be $(\frac{1}{2} - v_1)$: $(\frac{1}{2} + v_1)$ before taking into account the depopulation effects. The value of v_1 thus deduced is very close to zero.

B. Aluminum

In Fig. 14 we show lines 1 and 2 of aluminum acceptors in silicon with $\vec{F} \parallel \langle 111 \rangle$ for two stresses. The energies of the components as a function of stress are shown in Fig. 15. The sublevels of the Γ_8 ground state of aluminum are ordered in the same fashion as in Fig. 2(a) as deduced by OFR on the basis of the data for $2p'$ line. Accepting this ground-state ordering, the polarization features and the depopulation effects give the ordering of the excited state for lines 1 and 2 which are the same as that for boron. The ground-state spacing deduced from the spacing between 2.4 and 2.2 as well as that between 2.3 and 2.1 is shown in Fig. 16 as a function of stress; here the straight line represents a least-squares fit to the data points. From this we deduce a value of -3.84 ± 0.12 eV for d_0 of aluminum acceptors (see Table IV). We again attribute the nonlinearity in the stress dependence of 2.1, 2.3, and 1.4 to the mix-

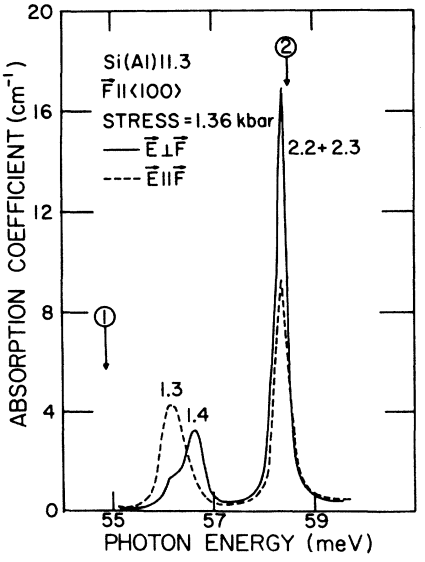

FIG. 17. Effect of a ⟨100⟩ compression on lines 1 and 2 of aluminum in silicon. $p(300\,^\circ\text{K}) = 2.7 \times 10^{15}$ cm^{-3}.

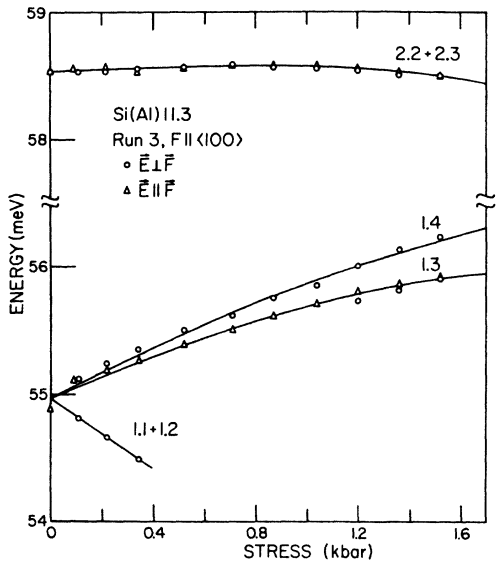

FIG. 18. Stress dependence of the energies of the stress-induced components of lines 1 and 2 of aluminum acceptors in silicon for $\vec{F} \parallel \langle 100 \rangle$. The solid curves passing through the data points represent second-degree polynomial fits.

ing of the $\Gamma_5 + \Gamma_6$ excited states of lines 1 and 2. The analysis of the data permits a determination of d_1, d_2, and $|V_{12}|/|T|$ for aluminum acceptors; these are included in Table IV. The mixing also results in marked changes in the intensity of 1.4 and 2.3 as a function of stress in a manner similar to that observed for boron; in Fig. 14, at the higher stress 1.4 has clearly gained in intensity relative to 1.3 and 2.3 has decreased with respect to 2.4. The available data were not extensive enough to permit an evaluation of u_1 and u_2.

The results for lines 1 and 2 of aluminum acceptors with $\vec{F} \parallel \langle 100 \rangle$ are shown in Fig. 17 while Fig. 18 contains the positions of the stress-induced components as a function of stress. As in the case of boron acceptors, 2.2 and 2.3 remained unresolved up to the maximum stress used and occurred close to the zero-stress position of line 2. Also, the polarization features are identical to those observed for boron, implying the level scheme in Fig. 2(b); thus $b_2 \approx -b_0$ and the failure to observe 2.1 and 2.4 requires that u_2 be very small. The component labeled 1.1+1.2 in Fig. 18 decreases in intensity with increasing stress as a result of depopulation effects. A consistent interpretation for the polarization features as well as the resolution of 1.3 and 1.4 for $\vec{E} \perp \vec{F}$ can be given if we accept the same level scheme as for line 2 in Fig. 2(b). The spacing between 1.3 and 1.1 yields the ground-state splitting which is shown in Fig. 16 as a function of stress. Note that in Fig. 16, the least-squares fits for $\vec{F} \parallel \langle 100 \rangle$ and $\vec{F} \parallel \langle 111 \rangle$ have the same slopes, within experimental error. This of course implies, as discussed in Sec. III, that the ground state of aluminum acceptor in silicon splits in an isotropic fashion for a given stress. In order to confirm this we examined the spectrum for $\vec{F} \parallel [110]$ and $\vec{q}$, the direction of light propagation, along $[1\bar{1}0]$. For this direction of stress, selection rules permit all the four components of lines 1 and 2 for both $\vec{E} \parallel \vec{F}$ and $\vec{E} \perp \vec{F}$. Figure 19 shows the experimental results; 1.1 and 1.4 represent transitions between the upper ground state and the lower excited state and between the lower ground state and the upper excited state, respectively. Depopulation effects show that the intermediate component 1.2 arises from the upper ground state to the upper excited state. Thus, the spacing between 1.4 and 1.2 gives the ground-state splitting, which is shown as a function of stress in Fig. 16. The slope of the least-squares fit to the data points agrees with those for $\vec{F} \parallel \langle 111 \rangle$ and $\vec{F} \parallel \langle 100 \rangle$ as demanded for stress isotropy. The deformation potential constant b_1 can be deduced from the spacing of 1.4 and 1.3 for $\vec{F} \parallel \langle 100 \rangle$ in Figs. 17 and 18. The deformation potential constants b_0, b_1, and b_2 are included in Table IV. It should be remarked here that the stress dependence of the components of line 1 for $\vec{F} \parallel \langle 110 \rangle$ do not show any nonlinear effects indicating the absence of mixing between the Γ_5 sublevels of the final states of lines 1 and 2.

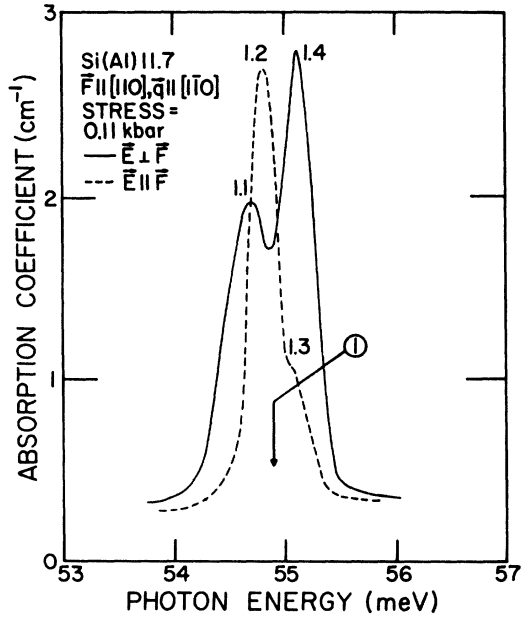

FIG. 19. Effect of a [110] compression on line 1 of aluminum acceptors in silicon. The direction of light propagation $\vec{q}$ is along $[1\bar{1}0]$; $p(300\,^\circ\text{K}) = 2.7 \times 10^{15}$ cm^{-3}.

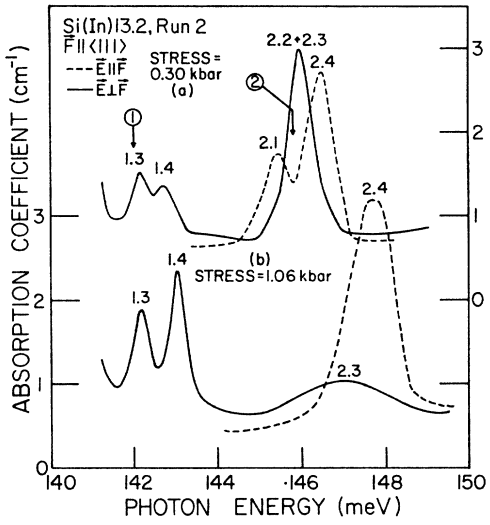

FIG. 20. Effect of a ⟨111⟩ compression on lines 1 and 2 of indium acceptors in silicon. $p(300\,^{\circ}\mathrm{K}) = 1.6\times10^{16}$ cm^{-3}. The somewhat larger widths of the components can be ascribed to the same reason as in Fig. 14.

C. Indium

The effect of uniaxial stress on lines 1 and 2 of indium acceptors in silicon is shown in Fig. 20 with $\vec{F} \parallel \langle 111\rangle$; the positions of components as a function of stress are shown in Fig. 21. The polarization features and the mixing effects are essentially identical to the case of boron acceptors and thus yield the same level scheme as shown in Fig. 2(a). In Fig. 22 we present the ground-state splitting as a function of stress; here the splitting was deduced from the spacing between 2.4 and 2.2 and from that between 2.3 and 2.1. From the data presented in Fig. 22 we deduce $d_0 = -2.68 \pm 0.15$ eV. The analysis of the results in Fig. 21, together with Eqs. (23)–(27), yields the values of d_1, d_2, and $|V_{12}|/|T|$ included in Table IV.

The effect of a compressive force $\vec{F} \parallel [110]$ and $\vec{q} \parallel [1\bar{1}0]$ is shown in Fig. 23. As mentioned earlier the selection rules permit all the transitions from the stress-induced ground-state sublevels to the excited-state sublevels. The line labeled 2.2+2.3 occurs close to the zero-stress positions of line 2. We ascribe this component to the transitions from the lower (higher) sublevel of the ground state to the lower (higher) sublevel of the excited state, the ground-state splitting being equal to the excited-state splitting. The spacing between 2.4 and 2.1 is thus twice the ground-state splitting. In Fig. 22 we show the ground-state splitting as a function

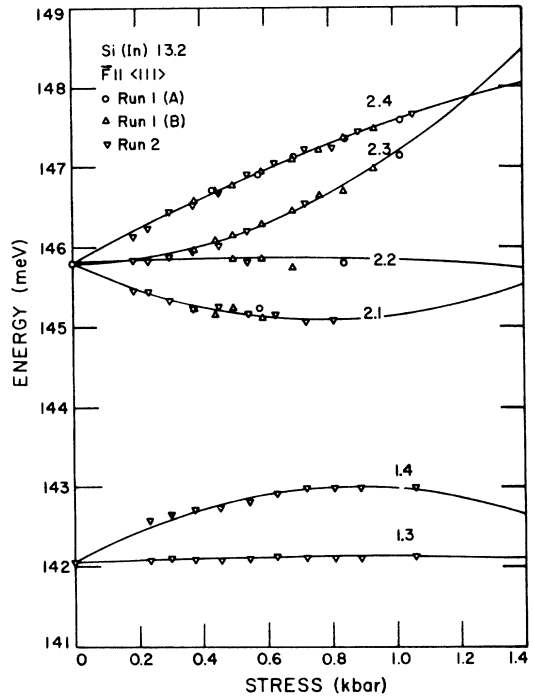

FIG. 21. Stress dependence of the energies of the components of line 1 and line 2 of indium in silicon for $\vec{F} \parallel \langle 111\rangle$. The solid curves passing through the data points represent second-degree polynomial fits by the method of least squares.

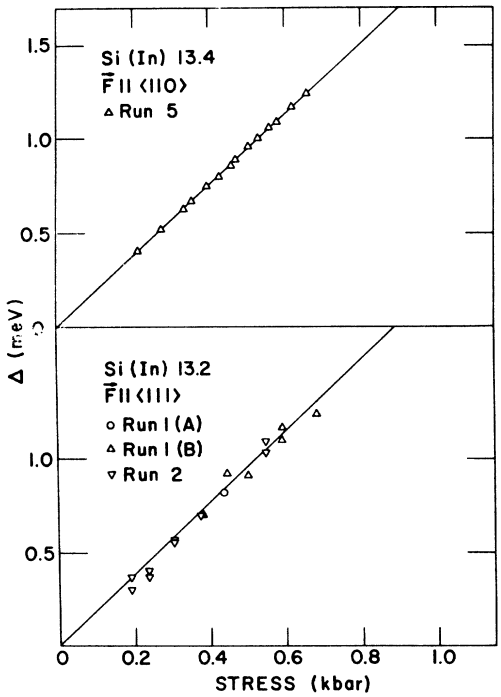

FIG. 22. Ground-state splitting Δ of indium acceptors in silicon as a function of stress with $\vec{F} \parallel \langle 111\rangle$ and ⟨110⟩. The values of Δ were obtained from the energy spacing (2.4 – 2.2) as well as (2.3 – 2.1) from Fig. 21 for $\vec{F} \parallel \langle 111\rangle$; for $\vec{F} \parallel \langle 110\rangle$, Δ was determined from $\frac{1}{2}$[2.4 – 2.1] (see Fig. 23 for a typical spectrum). The straight lines passing through the data points represent least-squares fits.

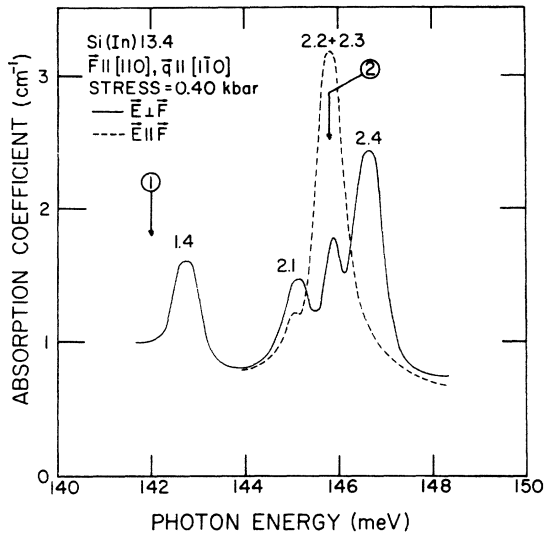

FIG. 23. Effect of a ⟨110⟩ compression on lines 1 and 2 of indium acceptors in silicon; $p(300\,^{\circ}\mathrm{K}) = 1.6\times10^{16}$ cm^{-3}.

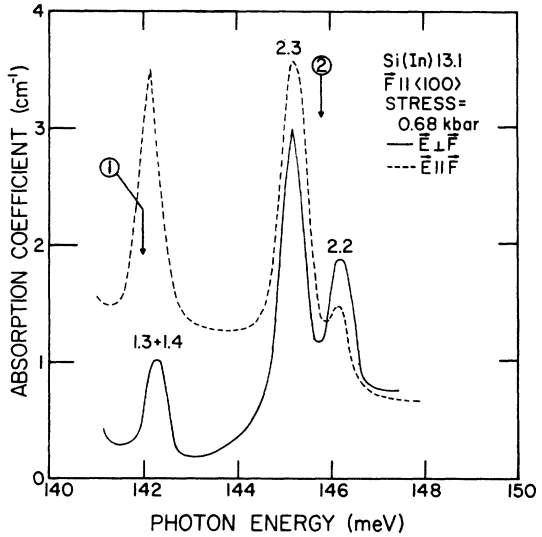

FIG. 24. Effect of a ⟨100⟩ compression on lines 1 and 2 of indium acceptors in silicon. $p(300\,^{\circ}\mathrm{K}) = 1.6\times10^{16}$ cm^{-3}.

of stress where the straight line represents a least-squares fit to the data points. The slopes for $\vec{F} \parallel \langle 111\rangle$ and $\vec{F} \parallel \langle 110\rangle$ are equal within experimental error. From Eq. (15) it can be seen that

$$4\Delta_{110}^2 = \Delta_{100}^2 + 3\Delta_{111}^2 \ . \tag{28}$$

Thus $|\Delta_{110}| = |\Delta_{111}|$, implies $|\Delta_{110}| = |\Delta_{100}| = |\Delta_{111}|$, i.e., stress isotropy for the ground-state splitting. The components of line 2 for $\vec{F} \parallel \langle 110\rangle$ do not exhibit any nonlinear stress dependence, again indicating the absence of mixing effects between the Γ_5 sublevels of the final states of lines 1 and 2.

The results for $\vec{F} \parallel \langle 100\rangle$ are presented in Figs. 24 and 25. The absence of 2.1 and 2.4 indicates that u_2 for indium, as for boron, is very small. A comparison of Figs. 13 and 25 reveals that the splitting of the excited state for indium is larger than that of the ground state, whereas these splittings are equal for boron. The component labeled 2.2 in Fig. 24 shows depopulation effects with increasing stress and hence arises from the upper sublevel of the ground state. The deformation potential constant b_0 can be obtained from the stress isotropy discussed above. It is not possible to deduce this directly from the $\vec{F} \parallel \langle 100\rangle$ measurements since 2.1 and 2.4 could not be observed and the $2p'$ line has not been studied; also, 1.1 and 1.2 could be observed only at moderate stresses due to the presence of the 9-μ oxygen band.[15] Accepting the ground-state splitting as deduced on the basis of stress isotropy, we can determine b_2 from the spacing between 2.2 and 2.3 which equals the difference between the excited-state splitting and the ground-state splitting; this gives $b_2 = 1.75 \pm 0.03$ eV. From the near coincidence of 1.3 and 1.4 in Fig. 25, the choice of the level ordering for the excited state can be that of line 1 or line 2 in Fig. 2(b), the excited-state splitting being nearly zero.

V. CONCLUDING REMARKS

The experimental results on the piezospectroscopic behavior of the group-III acceptors in sili-

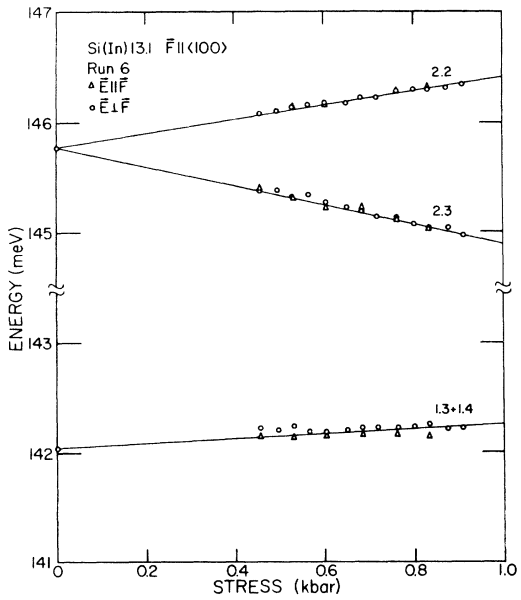

FIG. 25. Stress dependence of the energies of the stress-induced components of lines 1 and 2 of indium acceptors in silicon for $\vec{F} \parallel \langle 100\rangle$. The straight lines passing through the data points represent least-squares fits.

con reported in this paper are in excellent agreement with those of OFR. For $\vec{F} \parallel \langle 111 \rangle$, the ordering of the stress-induced sublevels of the ground and the first two excited states are unambiguously determined irrespective of whether the excited state of the $2p'$ line is of Γ_6 or Γ_7 symmetry. The interaction effects observed further substantiate the fact that the ordering of the excited-state sublevels of lines 1 and 2 are opposite, thus permitting a crossing of the $\Gamma_5+\Gamma_6$ states. The results for $\vec{F} \parallel \langle 100 \rangle$ confirm that the ground-state sublevels and the excited-state sublevels of line 2 are ordered oppositely; however, the actual symmetry of the sublevels may be the same as in Fig. 2(b) or reversed depending upon whether the final state of the $2p'$ line has Γ_6 or Γ_7 symmetry. The sign of b_0 is of course dependent on whether the ordering of the ground state is the same or opposite to that given in Fig. 2(b), the former yielding a negative sign and the latter a positive. Bir *et al.*[23] have deduced, using the results of Feher *et al.*,[24] that b_0 and d_0 are negative for silicon; this would imply the ordering of the ground-state sublevels given in Fig. 2(b) and in turn a Γ_6 symmetry for the final state of the $2p'$ line. As discussed in Sec. IV, the experimental results for $\vec{F} \parallel \langle 100 \rangle$ for line 1 imply a very small splitting for the final state; however all the evidence points to the conclusion that the ordering of the sublevels of the final state of line 1 is the same as that for line 2. The absence of interaction effects due to level crossing substantiates this further. It is also interesting to note that interaction effects were not observed for aluminum and indium acceptors with $\vec{F} \parallel \langle 110 \rangle$.

From Table IV it is clear that b_0 and d_0 for the three impurities studied show a chemical species dependence, the values decreasing with increasing ionization energy of the acceptor; this is not surprising since, as in the case of group-V donors, the ground state exhibits marked chemical shifts indicating the failure of the effective-mass theory. In fact it was deduced by Tekippe *et al.*[5] that the shear deformation-potential constant Ξ_u of the $1s(A_1)$ ground state of arsenic, phosphorus and antimony show a species dependence. On the other hand, Ξ_u of the excited p states of these impurities, and magnesium donors, was the same and equal to that of the $\langle 100 \rangle$ conduction-band minima of silicon. In contrast, the shear deformation-potential constants b_1 and b_2 of the excited states of lines 1 and 2 of boron, aluminum, and indium acceptors are reasonably close to one another but d_1 and d_2 are not. The differences in the zero-stress spectra of these acceptors already pointed out by OFR show that the effective-mass theory is not very successful even for the p-like state of silicon. In this context the differences in d_1's and d_2's for the impurities studied are not surprising. Bir *et al.*[23] and Suzuki *et al.*[25] have calculated the ratio b_0/b and d_0/d in the effective-mass approx-

TABLE V. Comparison of values of b and d for silicon determined by various methods.

Method		d (eV)	b (eV)	Temperature (°K)	Ref.
1. Piezospectroscopy of boron acceptors	(i)	-4.84 ± 0.10	-1.92 ± 0.05	~ 10	Present work[a]
	(ii)	-4.63 ± 0.10	-2.08 ± 0.05		
2. Piezospectroscopy of indirect exciton spectrum		-4.85 ± 0.15	-2.10 ± 0.10	77	b
3. Piezospectroscopy of indirect absorption edge		-5.30 ± 0.40	-2.40 ± 0.20	80	c
4. Band calculations		-5.7	-2.5	...	d
5. Cyclotron resonance of holes under uniaxial stress		-5.1 ± 0.9	-2.3 ± 0.4	1.25	e
6. Piezospectroscopic study of the 23-meV electronic Raman line of boron acceptors	(i)	-4.47 ± 0.12	-1.74 ± 0.06	liquid helium	f
	(ii)	-4.28 ± 0.12	-2.27 ± 0.06		
7. Heat-pulse propagation in p-type silicon under uniaxial stress.		-7.5 ± 0.8	-2.5 ± 0.3	~ 4	g

[a]Calculated using the b_0/b and d_0/d values of (i) Bir *et al.* (Ref. 23) and (ii) Suzuki *et al.* (Ref. 25).
[b]L. D. Laude, F. H. Pollak, and M. Cardona, Phys. Rev. B 3, 2623 (1971).
[c]I. Balslev, Phys. Rev. 143, 636 (1966).
[d]I. Goroff and L. Kleinman, Phys. Rev. 132, 1080 (1963).
[e]The values of d and b given here are from Ref. 31 as corrected by I. Balslev and P. Lawaetz, Phys. Lett. 19, 6 (1965).
[f]Calculated using the b_0/b and d_0/d values of (i) Bir *et al.* (Ref. 23) and (ii) Suzuki *et al.* (Ref. 25).
[g]See Ref. 27. We have given the average of the two values given by these authors.

imation; thus b and d can be, in principle, deduced from a knowledge of b_0 and d_0 for the impurity whose ionization energy is closest to the effective-mass value. Boron is the shallowest acceptor in silicon and has an ionization energy not too different from the effective-mass value[26]; b and d calculated from $b_0/b = 0.84$ and $d_0/d = 0.93$, the values given by Bir *et al.* and $b_0/b = 0.775$ and $d_0/d = 0.971$, the values of Suzuki *et al.*, are included in Table V, which compares the valence-band deformation-potential constants determined by various techniques. As can be seen our values are in excellent agreement with those obtained by other workers except those reported by Fjeldly *et al.*[27] Aggarwal and co-workers[28] obtain for boron, $b_0 = -1.46 \pm 0.06$ eV and $d_0 = -4.16 \pm 0.12$ eV from the effect of stress on the 23-meV electronic Raman line,[29] which are in good agreement with our values. Parsons[30] has also determined b_0 and d_0 from a quantitative piezospectroscopic study of the $2p'$ line of boron; his values differ from ours in a substantial manner for reasons not clear to us. As pointed out in Sec. III, the extrema of K occur along $\langle 100 \rangle$, $\langle 111 \rangle$, and $\langle 110 \rangle$, the absolute minima and maxima being along $\langle 100 \rangle$ and $\langle 111 \rangle$, respectively. Thus, the experimentally found equality $|\Delta_{100}| = |\Delta_{111}|$ tests the stress isotropy under the most stringent conditions. The stress isotropy of the ground-state splitting implies that b_0 and d_0 are not independent constants. It is interesting to note that this stress isotropy is observed for the three impurities investigated in the present work as well as for the top of the valence band.[31] A similar isotropy was observed by Thomas[32] for the valence band of CdTe. It is not clear at the present time whether this represents a physically interesting situation or it is only a fortuitous occurrence. The theoretical analysis used in this paper assumes a strain potential linear in strain and allows for only linear splittings and shifts except when interaction effects arise due to mixing. The results for lines 1 and 2, however, show nonlinear shifts of the center of gravity of the ground state and the results for the $2p'$ line of boron indicate that its final state also shifts in a nonlinear fashion.

ACKNOWLEDGMENTS

The authors wish to thank Miss Louise Roth for orienting the samples used in the present investigation. They are also indebted to Dr. R. L. Aggarwal for communicating the results quoted in the text.

---

*Work supported by the National Science Foundation (GH32001 and MRL Program GH33574) and the Advanced Research Projects Agency (IDL Program DAHC-0213).

[1]W. Kohn, *Solid State Physics*, edited by F. Seitz and D. Turnbull (Academic, New York, 1957), Vol. 5, p. 257.

[2]P. Fisher and A. K. Ramdas, *Physics of the Solid State*, edited by S. Balakrishna, M. Krishnamurthi, and B. Ramachandra Rao (Academic, New York, 1969), p. 149.

[3]H. P. Soepangkat and P. Fisher, Phys. Rev. B 8, 870 (1973).

[4]B. Pajot, F. Merlet, and G. Taravella, Can. J. Phys. 50, 2186 (1972); F. Merlet and B. Pajot (private communication); Y. Nisida and K. Horii, J. Phys. Soc. Jap. 31, 776 (1971); K. Horii and Y. Nisida, J. Phys. Soc. Jap. 31, 783 (1971).

[5]V. J. Tekippe, H. R. Chandrasekhar, P. Fisher, and A. K. Ramdas, Phys. Rev. B 6, 2348 (1972).

[6]F. Barra, P. Fisher, and S. Rodriguez, Phys. Rev. B 7, 5285 (1973).

[7]H. R. Chandrasekhar, P. Fisher, A. K. Ramdas, and S. Rodriguez, Phys. Lett. A 41, 137 (1972).

[8]R. L. Jones, Ph.D. thesis (Purdue University, 1968) (unpublished).

[9]Perkin Elmer Corp. Norwalk, Connecticut.

[10]A. Mitsuishi, Y. Yamada, S. Fujita, and H. Yoshinaga, J. Opt. Soc. Am. 50, 433 (1960).

[11]Samples Si(B)4 and Si(B)8 were obtained from Semi-Elements Inc., Saxonburg, Pa. All others were obtained from Texas Instruments, Inc., Dallas, Texas 75222.

[12]G. F. Koster, J. O. Dimmock, R. G. Wheeler, and H. Statz, *Properties of the Thirty-two Point Groups* (MIT U. P., Cambridge, Massachusetts, 1966).

[13]See Ref. 10 in A. K. Bhattacharjee and S. Rodriguez, Phys. Rev. B 6, 3836 (1972).

[14]R. J. Elliot, Phys. Rev. 96, 266 (1954).

[15]A. Onton, P. Fisher, and A. K. Ramdas, Phys. Rev. 163, 686 (1967).

[16]In the effective-mass approximation the impurity wave function is written in the form $F_{i\mu}(\vec{r})\psi_i(\vec{r})$, where $\psi_i(\vec{r})$ is a Bloch function of a $p_{3/2}$ ($p_{1/2}$) state at $k = 0$ and $F_{i\mu}(\vec{r})$, is the envelope wave function of the μth state associated with the ith band. The matrix element for dipole transition from the $i\mu$ to the $j\nu$ level is $\int d\vec{r} F^*_{j\nu}(\vec{r})\psi^*_j(\vec{r})\vec{r}F_{i\mu}(\vec{r})\psi_i(\vec{r})$. If the envelope function is essentially constant over each primitive cell the above integral can be approximated by

$$(1/\Omega_0)\int_{\text{crystal}} F^*_{j\nu}(\vec{r})F_{i\mu}(\vec{r})\,d\vec{r}\int_{\text{primitive cell}}\psi^*_j(\vec{r})\vec{r}\,\psi_i(\vec{r})\,d\vec{r}$$

$$+ (1/\Omega_0)\int_{\text{primitive cell}}\psi^*_j(\vec{r})\psi_i(\vec{r})\,d\vec{r}\int_{\text{crystal}} F^*_{j\nu}(\vec{r})\vec{r}\,F_{i\mu}(\vec{r})\,d\vec{r}.$$

Here Ω_0 is the volume of the primitive cell. The first integral of the second term vanishes if i and j are different band states. However, the second integral of the first term also vanishes since it represents the dipole matrix element of a $p_{3/2}$ to $p_{1/2}$ transition in the pure crystal. [See E. O. Kane, J. Phys. Chem. Solids 1, 83 (1956).] On the other hand, if $i = j$, the second term yields the selection rule for the $p_{3/2}$ series. The experimental observation of the $p_{1/2}$ series implies that the above approximation is inadequate. (See also Ref. 26.)

[17]See, for example, S. Rodriguez, P. Fisher, and F. Barra, Phys. Rev. B 5, 2219 (1972).

[18]From Unsöld's theorem, $\psi_1^\dagger\psi_1 + \psi_2^\dagger\psi_2$ belongs to Γ_1 and from the time reversal invariance of V, $\langle\psi_1 | V | \psi_1\rangle = \langle\psi_2 | V | \psi_2\rangle$. Since $\Gamma_6 \times \Gamma_6 = \Gamma_1 + \Gamma_4$, the off-diagonal matrix elements of V in a basis which generates Γ_6 vanish.

[19]Since $J_xJ_y - J_yJ_x = iJ_z$, $\mathrm{Tr}J_z = 0$; $\mathrm{Tr}J_x^2 = \mathrm{Tr}J_y^2 = \mathrm{Tr}J_z^2$

$= (1/3)\mathrm{Tr}J^2 = 5$. Note $J_x^2/2 + J_y^2/2 + \{J_xJ_y\}$ is the square of the projection of $\vec{J}$ along the [110] axis and thus has trace 5. Therefore $\mathrm{Tr}\{J_xJ_y\} = 0$.

[20]The term $u_1(u_2)$ in Table III refers to the single parameter characterizing the relative intensities of the stress-induced components of line 1(2) when $\vec{F} \parallel \langle 111 \rangle$. For a formal definition of this parameter see Eqs. (72) and (73) of Ref. 13. The symbols N_1 and N_2 stand for the zero-stress intensities of lines 1 and 2, respectively.

[21]In Refs. 15 and 17 (Table XIV) it has been shown that for $\Gamma_8 \rightarrow \Gamma_6$ or Γ_7, the relative intensities of the two stress induced components are in the ratio 3:1:4 for $(\Gamma_5 + \Gamma_6 \rightarrow \Gamma_4)_\perp$: $(\Gamma_4 \rightarrow \Gamma_4)_\perp$: $(\Gamma_4 \rightarrow \Gamma_4)_\parallel$ when $\vec{F} \parallel \langle 111 \rangle$; the same ratios are obtained for $(\Gamma_6 \rightarrow \Gamma_6)_\perp$: $(\Gamma_7 \rightarrow \Gamma_6)_\perp$: $(\Gamma_7 \rightarrow \Gamma_6)_\parallel$ when $\vec{F} \parallel \langle 100 \rangle$. Experimentally, the relative intensities are consistent with these predictions. What is interesting, however, is that the ratio of the intensities of $[2p'(-)]_\perp$: $[2p'(+)]_\perp$: $[2p'(+)]_\parallel$ for $\vec{F} \parallel [110]$ is also 3:1:4. From Figs. 4 and 5 of Ref. 17 it can be immediately seen that $|\Delta_{111}| = |\Delta_{100}|$ and stress isotropy follows.

[22]J. J. Hall, Phys. Rev. 161, 756 (1967). Liquid-helium values of $s_{44} = 1.246 \times 10^{-3}$/kbar and $s_{11} - s_{12} = 9.745 \times 10^{-4}$/kbar have been used to evaluate the deformation-potential constants.

[23]G. L. Bir, E. I. Butikov, and G. E. Pikus, J. Phys. Chem. Solids 24, 1467 (1963).

[24]G. Feher, J. C. Hensel, and E. A. Gere, Phys. Rev. Lett. 5, 309 (1960).

[25]K. Suzuki, M. Okazaki, and H. Hasegawa, J. Phys. Soc. Jap. 19, 930 (1964).

[26]K. S. Mendelson and D. R. Schultz, Phys. Status Solidi 31, 59 (1969).

[27]T. Fjeldly, T. Ishiguro, and C. Elbaum, Phys. Rev. B 7, 1392 (1973).

[28]R. L. Aggarwal (private communication). J. M. Cherlow, R. L. Aggarwal, and B. Lax, Phys. Rev. B 7, 4547 (1973).

[29]G. B. Wright and A. Mooradian, Phys. Rev. Lett. 18, 608 (1967).

[30]R. R. Parsons, Ph. D. thesis (University of British Columbia, 1968) (unpublished).

[31]J. C. Hensel and G. Feher, Phys. Rev. 129, 1041 (1963).

[32]D. G. Thomas, J. Appl. Phys. 32, 2298 (1961).